JACS
JOURNAL OF THE AMERICAN CHEMICAL SOCIETY
Article
pubs.acs.org/JACS

Molecular-Level Characterization of the Breathing Behavior of the Jungle-Gym-type DMOF-1 Metal–Organic Framework

Jason S. Grosch and Francesco Paesani*

Department of Chemistry and Biochemistry, University of California, San Diego, 9500 Gilman Drive, La Jolla, California 92093, United States

Supporting Information

ABSTRACT: Fundamental insights into the molecular mechanisms that determine the breathing behavior of the jungle-gym-type DMOF-1 metal–organic framework upon adsorption of benzene and isopropyl alcohol are gained from computer simulations. In all cases, good agreement is obtained between the calculated and experimental structural parameters. In the case of benzene adsorption, DMOF-1 is predicted to exist in a narrow pore configuration at high loadings and/or low temperature. A structural transition into a large pore configuration is then observed as the temperature increases and/or the loading decreases, which is directly related to the spatial distribution and molecular interactions of the benzene molecules within the pores. The isopropyl alcohol adsorption simulations indicate that DMOF-1 undergoes two distinct structural transitions (from large pore to narrow pore and then back to large pore) as the number of adsorbed molecules increases, which is explained in terms of the formation of hydrogen bonds between the isopropyl molecules and the framework.

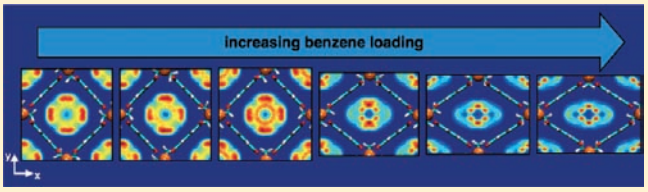

1. INTRODUCTION

Over the past decade, metal–organic frameworks (MOFs) have emerged as a new class of porous materials with great potential for a wide range of applications, including catalysis, separation, and gas storage (e.g., see refs 1–4 and references therein). MOFs are made of inorganic and organic subunits, with the organic molecules acting as linkers between metal clusters that serve as nodes.[5] The enormous number of possible combinations between these subunits has allowed for the synthesis of a large number of MOF structures with highly specific properties.[6−18] In particular, it has been shown that the size, shape, and physicochemical characteristics of the pores can be rationally tuned by varying the organic linkers and/or the metal clusters.[19]

Unlike traditional porous materials, such as zeolites, several MOFs are characterized by unusually flexible frameworks that undergo large structural deformations upon external stimuli such as temperature or pressure changes, and gas adsorption.[3,20−28] These structural deformations are generally associated with a reversible transition from large to narrow pore structures, which results in the so-called breathing behavior. Experimentally, the breathing effect induced by guest molecules is correlated with the appearance of both steps and hysteresis in the corresponding adsorption/desorption isotherms. To date, guest-induced breathing has been observed in several MOFs that have attracted much interest because of their potential role in the development of functional materials for gas separation and sensing.[20,21,23,24,26,27,29−32] Among MOFs that can breathe, MIL-53 is certainly the most studied structure.[21,30,33−35] It has been shown that the unit cell of MIL-53 crystals can shrink up to 32% in volume upon hydration,[21] and well-defined steps and hysteresis have been observed in the CO_2 adsorption/desorption isotherms.[30]

More recently, it has been demonstrated that the breathing effect can also be modulated by chemical functionalization of the framework.[32,36,37] In this regard, a covalent postsynthetic modification strategy has been used to modify the framework of DMOF-1–NH_2, an amino derivative of DMOF-1.[32] DMOF-1 is a three-dimensional, jungle-gym-type MOF that breathes upon adsorption of benzene or isopropyl alcohol (IPA), but remains rigid with CO_2 and H_2.[20,38−40] The introduction of short alkyl chains through postsynthetic modification yields significantly lower adsorptions of N_2 and CO_2 as compared to the unmodified material, a result that has been attributed to the decrease in pore volume.[32]

The molecular-level characterization of the breathing behavior is particularly relevant for the rational design of new MOF structures with properties specifically tailored for gas separation and sensing. In this context, computer simulations can play an important role by enabling the identification of the molecular interactions and physical mechanisms that determine the observed structural deformations. However, most of the computational studies on MOFs reported so far in the literature have focused primarily on the modeling of gas adsorption in connection with the corresponding experimental measurements. Very little is ascertained about the intrinsic properties of the framework itself. With few exceptions,[30,35,41] all previous simulations have been performed on MOF structures that are

Received: October 26, 2011
Published: February 7, 2012

 © 2012 American Chemical Society dx.doi.org/10.1021/ja2100615 | J. Am. Chem. Soc. 2012, 134, 4207–4215

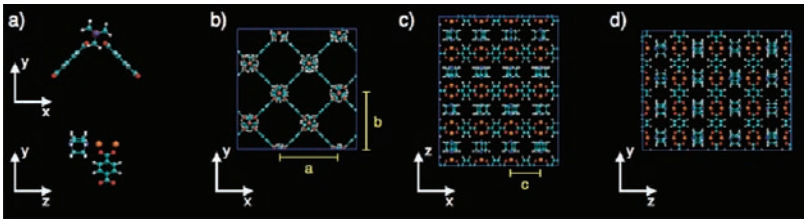

Figure 1. (a) DMOF-1 unit cell projected into the $x-y$ (top) and $z-y$ (bottom) planes; (b) DMOF-1 three-dimensional structure projected into the $x-y$ plane; and (c) DMOF-1 three-dimensional structure projected into the $z-y$ plane. Zn, orange; C, cyan; O, red; H, white; N, blue. Also indicated in yellow are the three unit cell parameters a, b, and c.

experimentally known not to breathe or under conditions in which breathing is suppressed. In these particular cases, the assumption of a rigid structure generally leads to good agreement with the available experimental data. For example, the adsorption of CO_2 and N_2 in DMOF-1 has recently been modeled assuming a completely rigid framework.[38,42]

Treating MOFs as rigid structures obviously provides an incomplete description of the structural properties of these materials and prevents the characterization of the framework flexibility that is associated with the breathing effect. A physically realistic model of the MOF properties should allow the framework to be completely flexible to adjust accordingly in response to any external stimuli such as gas adsorption or temperature/pressure changes. To our knowledge, flexible models for MOFs that breathe have been developed only for MIL-53(Cr),[30,35] whose breathing behavior upon adsorption of CO_2,[30] H_2S,[34] and H_2O[35] has recently been investigated through computer simulations. On the basis of calculations carried out using density functional theory (DFT), it has been argued that weak dispersion interactions can play an important role in the breathing behavior of MOFs induced by guest molecules.[43,44] A theoretical description of the breathing effect based on thermodynamic principles has also been proposed,[45−47] while different simulation approaches have been developed to calculate both cell shape and size of MOF structures loaded with guest molecules at 0 K.[48]

To provide fundamental molecular-level insights into the breathing behavior of MOFs, we describe here the first fully flexible model of DMOF-1. In the new model, all of the interactions are described in terms of a molecular mechanics force field derived from ab initio data. Molecular dynamics (MD) simulations are then used to investigate the breathing behavior of DMOF-1 upon adsorption of benzene and isopropyl alcohol. In both cases, good agreement (which is quantitative in the case of benzene adsorption) with the available experimental data is obtained. Importantly, the simulation results allow for the characterization of the molecular mechanisms that lead to the structural deformation of the framework with chemically different guest molecules as a function of both loading and temperature. Besides providing new insights into the flexibility of DMOF-1, this study also represents the first step toward the characterization of the breathing behavior induced by postsynthetic modifications of the DMOF-1 framework.[32,37]

This Article is organized as follows: The computational approach is presented in section 2, the results are discussed in section 3, and the conclusions are given in section 4.

2. COMPUTATIONAL METHODOLOGY

The structure of DMOF-1 (molecular formula $Zn_2(BDC)_2DABCO$) consists of BDC (1,4-benzenedicarboxylate) ligands that are bound to Zn atoms to form two-dimensional grids (Figure 1a). The latter are then interconnected through the DABCO (1,4-diazabicyclo[2,2,2]-octane) ligands, which results in the overall three-dimensional pillared paddle-wheel structure (Figure 1b−d). A fully flexible force field is developed here and applied to the investigation of the breathing behavior of DMOF-1 upon adsorption of benzene and isopropyl alcohol, for which experimental data are available.[20,39,40] The General Amber Force Field (GAFF)[49] is used to model the intramolecular interactions within the two organic ligands, while specific parametrizations of the interactions between the metal units and the organic ligands are instead derived from fits to the corresponding ab initio data.

2.1. Ab Initio Calculations and Force Field Development. The ab initio calculations were performed using Gaussian 09,[50] and the molecular fragments shown in Figures 2 and 3 were used to model the

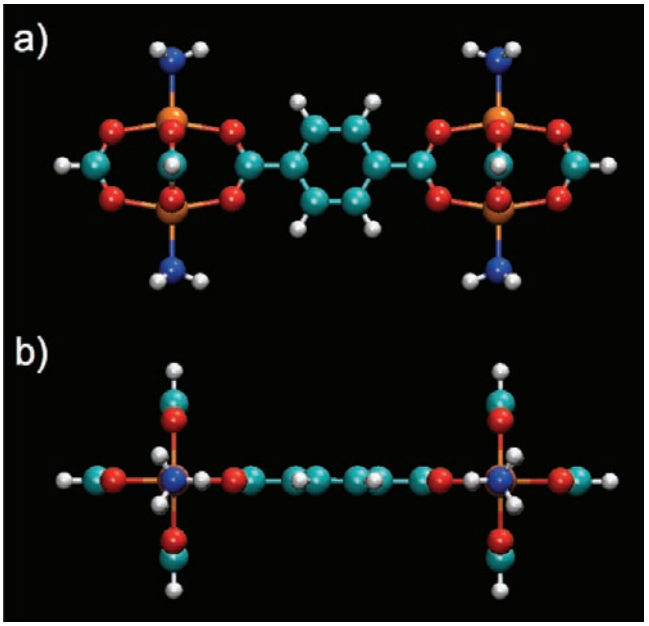

Figure 2. Top (a) and side (b) views of the framework fragment including one BDC ligand between two metal units, $[Zn_2(HCO_2)_3]$, which was used in the ab initio calculations. Each Zn atom was capped with one $-NH_3$ group to mimic the actual environment found in DMOF-1. See text for details.

electronic structure of DMOF-1. In both cases, to mimic the electrostatic environment present in DMOF-1, the Zn atoms were capped with $-NH_3$ groups positioned at a distance of 2.074 Å, corresponding to the experimental Zn−N distance. A detailed analysis of the structural and electrostatic properties of both fragments was initially carried out using density functional theory with the M062X[51] and B3LYP[52] hybrid functionals. The cc-pVDZ basis set[53] was used for the C, O, and H atoms, while both the LANL2DZ[54] and cc-pVDZ-PP[55] basis sets were used for the Zn atoms. The comparison of the results obtained with the two functionals, which is reported in the

dx.doi.org/10.1021/ja2100615 | J. Am. Chem. Soc. 2012, 134, 4207−4215

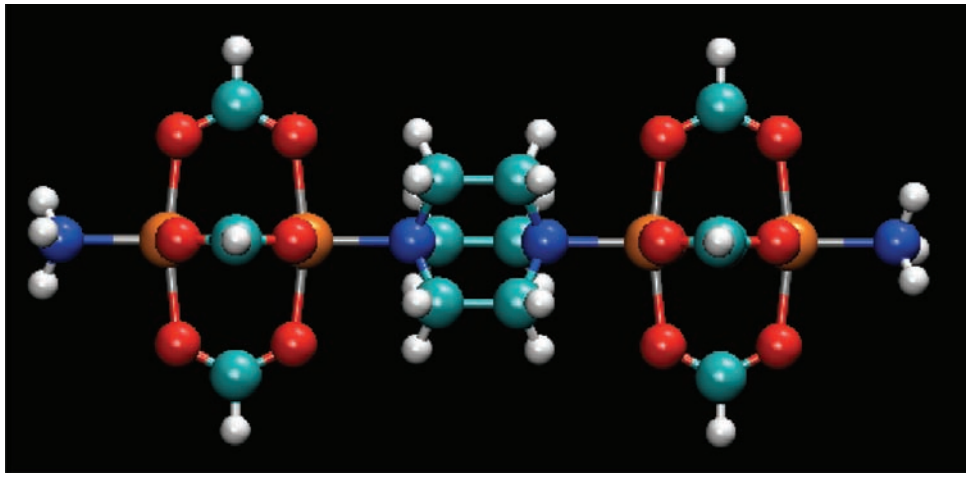

Figure 3. Framework fragment including one DABCO ligand between two metal units, $[Zn_2(HCO_2)_3]$, which was used in the ab initio calculations. Each of the outer Zn atoms was capped with one $-NH_3$ group to mimic the actual environment found in DMOF-1. See text for details.

Supporting Information, indicates that M062X most accurately reproduces the experimental structural data. On the basis of this analysis, all ab initio calculations required to determine the parameters of the new flexible DMOF-1 force field were carried out using the M062X functional with the cc-pVDZ (for H, C, N, and O) and cc-pVDZ-PP (for Zn) basis sets.

First, an energy minimization was performed for the fragment shown in Figure 2, which includes one BDC ligand between two truncated metal units $[Zn_2(HCO_2)_3]$. The resulting optimized structure was used to determine the BDC atomic partial charges from the fit to the calculated electrostatic potential using the CHELPG method.[56] The parameters associated with the potential functions that describe the interaction between the metal units and the BDC ligands were determined from fits to the corresponding ab initio data calculated as a function of the relevant coordinates (see the Supporting Information for specific details). The atomic partial charges of the DABCO ligands were determined following a two-step procedure. In the first step, the energy minimization of the isolated DABCO ligand was performed. The resulting structure was placed between two truncated metal units (Figure 3), and M062X calculations were carried out to optimize the Zn−N distances within the molecular fragment. The atomic partial charges for the entire fragment were fitted to the calculated electrostatic potential using the CHELPG method.[56] Following the same procedure used for the BDC ligands, the parameters associated with the potential functions describing the interactions between the metal units and the DABCO ligands were determined from the fit to the corresponding ab initio data calculated as a function of the relevant coordinates. The fitting process also included a bond between the Zn atoms belonging to the same metal unit, which was added to overcome the unrealistically strong repulsion that results from a force field description of the electrostatic interactions in terms of point charges. Similar bonds were also included in the force field used to model the HKUST-1 framework, a paddle-wheel metal−organic framework as DMOF-1.[57] It is important to note that the force constants associated with the Zn−O and Zn−N bonds, which effectively bind the BDC and DABCO ligands to the metal units, are relatively weak. This suggests that both ligands may be displaced by guest molecules that can interact strongly with the Zn atoms (e.g., water), which can be related to the observed instability of DMOF-1 under humid conditions.[58] The remaining nonbonded interactions were described by Lennard-Jones potentials using the corresponding GAFF parameters. The computational details of the fitting procedure are reported in the Supporting Information.

The benzene force field was taken from refs 59 and 60 because it was shown to accurately reproduce high-level ab initio data for the benzene−benzene dimer. A specific force field was instead developed for isopropyl alcohol. The IPA atomic partial charges were determined from a fit to the ab initio electrostatic potential calculated with the M062X functional using the CHELPG method. Both intramolecular and Lennard-Jones interactions were described using the corresponding GAFF parameters. No attempt was made to further optimize the IPA force field because such parametrization lies outside the scope of the present study. The complete list of the force field parameters is reported in the Supporting Information.

2.2. MD Simulations. All molecular dynamics simulations were performed with DL_POLY4[61] on a DMOF-1 structure consisting of 32 unit cells with periodic boundary conditions (Figure 1b−d). The short-range interactions were truncated at an atom−atom distance of 10.0 Å, while the electrostatic interactions were treated using the smooth particle mesh Ewald method.[62] Three different systems were considered: evacuated DMOF-1, DMOF-1 with a variable number of benzene molecules per unit cell (N_{BENZ} = 0.25−3.00), and DMOF-1 with a variable number of isopropyl alcohol molecules per unit cell (N_{IPA} = 1.00−5.00). In all calculations, the guest molecules were initially distributed uniformly in the nanopores, and each system was allowed to relax during a molecular dynamics simulation of 500 ps carried out in the canonical (NVT) ensemble. The production runs were then performed in the constant stress and constant temperature ($N\sigma T$) ensemble, and all properties were averaged over 3 ns. The temperature and pressure were maintained via Langevin dynamics with thermostat and barostat relaxation times of 1 and 5 ps, respectively. The equations of motion were propagated according to the velocity−Verlet algorithm with a time step of 1 fs.[62]

3. RESULTS AND DISCUSSION

3.1. Temperature Effects at Constant Benzene Loading. $N\sigma T$ simulations were initially performed for the evacuated DMOF-1 structure at T = 223 K that corresponds to the temperature used in the experiments of ref 20. The calculated lattice parameters are $a = b$ = 15.5 ± 0.2 Å and c = 9.6 ± 0.1 Å, which are in quantitative agreement (within the statistical uncertainty) with the corresponding crystallographic values $a = b$ = 15.4556 Å and c = 9.6715 Å.[20] A second set of simulations was carried out to characterize the structural changes of the framework induced by benzene adsorption. To make a direct comparison with the available experimental data,[20] MD simulations in the $N\sigma T$ ensemble were performed at T = 223 K with two benzene molecules per unit cell. These simulations predict lattice parameters that are in excellent agreement with the corresponding experimental data. The lengths of the a, b, and c unit cell vectors are, respectively, 16.9 ± 0.3, 13.8 ± 0.3, and 9.69 ± 0.06 Å, which reproduce (within

dx.doi.org/10.1021/ja2100615 | J. Am. Chem. Soc. 2012, 134, 4207−4215

the statistical uncertainty) the corresponding crystallographic values of 17.0664, 13.5004, and 9.6715 Å.

Using the same setup (DMOF-1 with two benzene molecules per unit cell), molecular-level insights into the structural changes of the framework induced by benzene adsorption were obtained from $N\sigma T$ simulations carried out at different temperatures. Figure 4 shows the variation of the unit cell

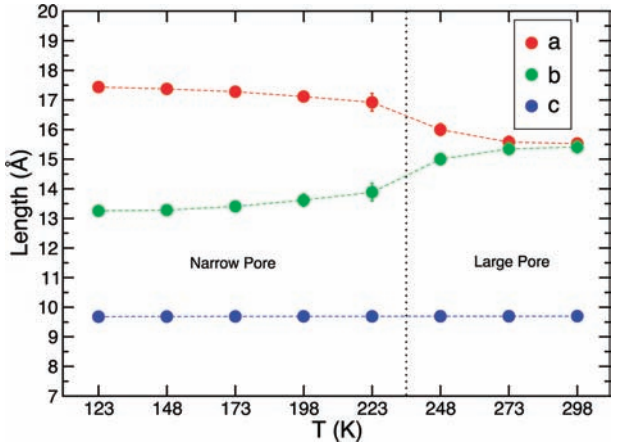

Figure 4. Variation of the unit cell vectors of DMOF-1 with two benzene molecules adsorbed per unit cell as a function of the temperature. The black dotted line indicates approximately the transition temperature from a narrow pore to a large pore structure.

vectors between T = 123 K and T = 298 K. Below T = 200 K, the pore size is predicted to be slightly narrower than that obtained at T = 223 K, which can be related to the reduced mobility of the benzene molecules as well as to the increased rigidity of the framework at low temperature. By contrast, a pronounced variation in the length of the unit cell vectors is observed at higher temperatures, with the DMOF-1 structure effectively stabilizing into the large pore (LP) configuration at $T \geq$ 248 K.

To quantitatively characterize the molecular mechanisms that are responsible for the observed breathing behavior of DMOF-1 as a function of temperature, the spatial distribution of the benzene molecules within the pores was also analyzed. Figure 5 shows a series of two-dimensional (2-D) density maps obtained by projecting the coordinates of the carbon atoms of each benzene molecule into the $x-y$ (left panels), $x-z$ (middle panels), and $z-$y (right panels) planes defined in Figure 1. At T = 123 K, it is possible to clearly identify six spots on the $x-y$ plane corresponding to the six carbon atoms of the benzene molecules. Two high-density regions are also found in correspondence of the bottom and top corners of the framework channels formed by the BDC ligands and the metal units on the $x-y$ plane. Inspection of the three different density maps indicates that the spatial arrangement of the benzene molecules at low temperature is highly ordered, with one-half of the molecules located at the center of the channels in correspondence of the BDC ligands with the aromatic ring lying on the $x-y$ plane. These molecules effectively act as gates that separate the individual pores and lead to the formation of closed compartments along the channels. The remaining molecules are instead located in the proximity of the DABCO ligands with the aromatic ring lying on the $x-z$ plane. As the temperature increases, the arrangement of the benzene molecules within the pores becomes increasingly more

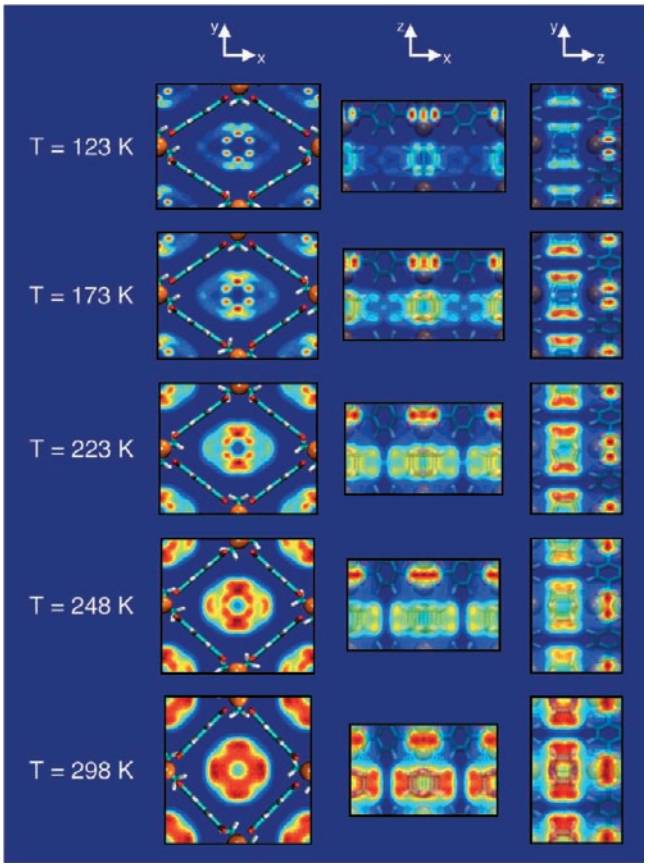

Figure 5. Two-dimensional density maps obtained at different temperatures by projecting the coordinates of the carbon atoms of each benzene molecule into the $x-y$ (left panels), $x-z$ (middle panels), and $z-y$ (right panels) planes that are defined in Figure 1. The density is normalized to the maximum value for each panel, and the color scheme varies from blue = 0.0 to red = 1.0.

disordered. At T = 298 K, four high-density regions are found on the $x-y$ plane at the four corners of the framework channels. These regions represent benzene molecules that lie on $x-z$ and $z-y$ planes. A more uniform distribution of the benzene molecules is found at the center of the channels, which can be associated with the increased molecular mobility at high temperatures. From the analysis of the two-dimensional density maps, it is possible to locate the transition between ordered and disordered arrangements of the benzene molecules in the temperature range 223 K < T < 248 K, which directly correlates with the temperature dependence of the lattice parameters shown in Figure 4. Shown in Figure 6 are snapshots taken from $N\sigma T$ simulations at three different temperatures that illustrate the preferential position of the benzene molecules inside the DMOF-1 channels.

The spatial arrangement of the benzene molecules obtained from simulations at T = 223 K is in agreement with the structural information derived from the crystallographic data of ref 20. This provides support for the accuracy of the present simulations in describing the molecular mechanisms that are responsible for the breathing behavior of DMOF-1 upon benzene adsorption. In this regard, the results reported in Figures 4 and 5 indicate that, for an average of two benzene molecules per unit cell, the transition from the large to the narrow pore (NP) structure is effectively determined by the interactions between the benzene molecules and the aromatic

dx.doi.org/10.1021/ja2100615 | J. Am. Chem. Soc. 2012, 134, 4207–4215

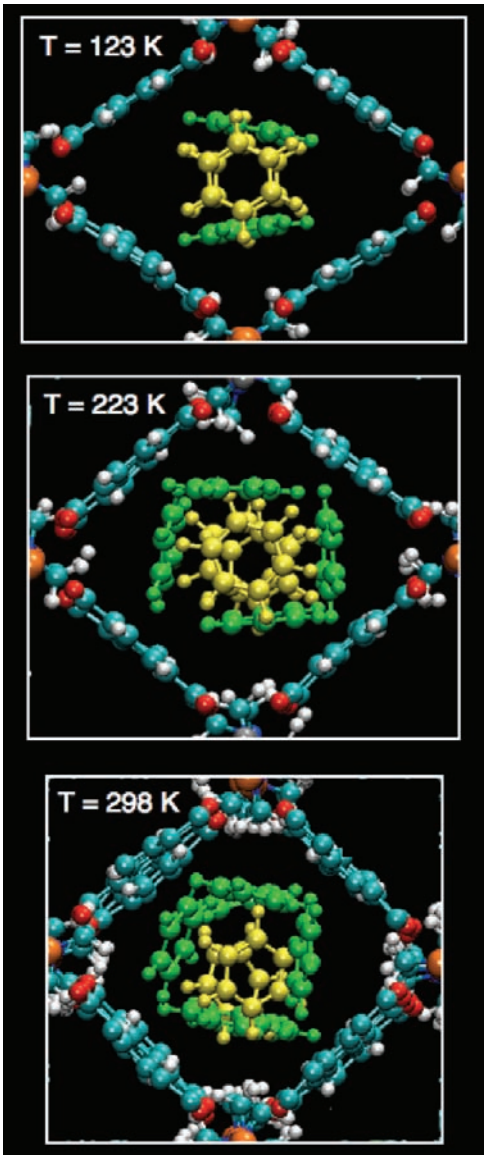

Figure 6. Three-dimensional snapshots along the *c* axis taken from *NσT* simulations of DMOF-1 with two benzene molecules per unit cell at three different temperatures. The benzene molecules lying on the *x*−*y* plane are shown in yellow, while those lying parallel to the *c* axis are shown in green. The same color scheme as in Figure 1 is used for the atoms of the framework.

rings of the BDC ligands. Considering the similarity between the BDC ligands and the benzene molecules, the particular arrangement of the latter within the DMOF-1 pores effectively reproduces the T-shape conformation of the benzene dimer, which has been shown to correspond to the lowest energy conformation for two benzene molecules.[60] The structural transition observed in the temperature interval 198 K < *T* < 273 K is thus the result of a subtle balance between the strength of the molecular interactions, which can be related to the enthalpic contribution to the free energy describing the transition process, and the increased disorder associated with the available thermal energy, which can be instead related to the entropic contribution to the free energy.

3.2. Benzene Loading Effects at Constant Temperature. The deformation of the DMOF-1 structure induced by benzene was also analyzed as a function of the number of molecules adsorbed per unit cell. The variation of the unit cell vectors as a function of N_{BENZ} shown in Figure 7 clearly

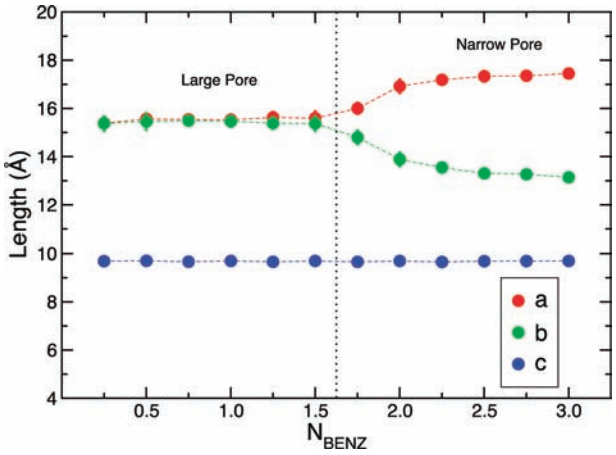

Figure 7. Variation of the unit cell vectors of DMOF-1 at *T* = 223 K as a function of the number of benzene molecules adsorbed per unit cell. The black dotted line indicates approximately the number of benzene molecules per unit cell that are approximately required to induce the transition from a narrow pore to a large pore structure.

indicates that at low loadings the most stable DMOF-1 structure corresponds to the large pore configuration. The transition into the narrow pore structure is predicted to occur approximately between N_{BENZ} = 1.50 and N_{BENZ} = 1.75. The variation of the pore size with N_{BENZ} can be directly related to the spatial distribution of the benzene molecules within the pore, which is analyzed in Figure 8 in terms of the 2-D density maps calculated for N_{BENZ} = 0.5−3.0. In the open configuration found at low loadings, the benzene molecules are preferentially located at the corners of the framework channels. Up to N_{BENZ} = 1.50, the molecules effectively lie on the walls of the channels with their molecular planes parallel to the channels axis. The structural transition is directly connected to the formation of gated compartments along the channels, which first appear at $N_{BENZ} \approx 1.75$ and are well-defined at N_{BENZ} = 2.00, with one-half of the benzene molecules now lying on the *x*−*y* plane. A further slight reduction of the pore size is observed between N_{BENZ} = 2.00 and N_{BENZ} = 3.00. At this loading, each benzene within a unit cell molecule lies, on average, on one of the three planes (*x*−*y*, *x*−*z*, and *z*−*y*). This particular arrangement leads to two different types of interactions between the benzene molecules and the framework, which both contribute to the reduction of the pore size. The first and major contribution arises from the interactions of the benzene molecules lying on the *x*−*y* plane with the aromatic rings of the BDC ligands, which is responsible for the initial reduction of the pore size at $N_{BENZ} \approx 1.75$. The second contribution involves the benzene molecules lying on the *x*−*z* and *z*−*y* planes. These molecules are located preferentially at the corners of the framework channels where they interact primarily with the DABCO ligands. The different spatial distribution of the benzene molecules as a function of loading can be clearly seen in Figure 9, which reports snapshots taken from *NσT* simulations with N_{BENZ} = 1.0, 2.0, and 3.0 showing the three-dimensional arrangement of the molecules inside the DMOF-1 pores viewed along the *c* axis.

3.3. Isopropyl Alcohol Loading Effects at Constant Temperature. To characterize at the molecular level the

dx.doi.org/10.1021/ja2100615 | J. Am. Chem. Soc. 2012, 134, 4207−4215

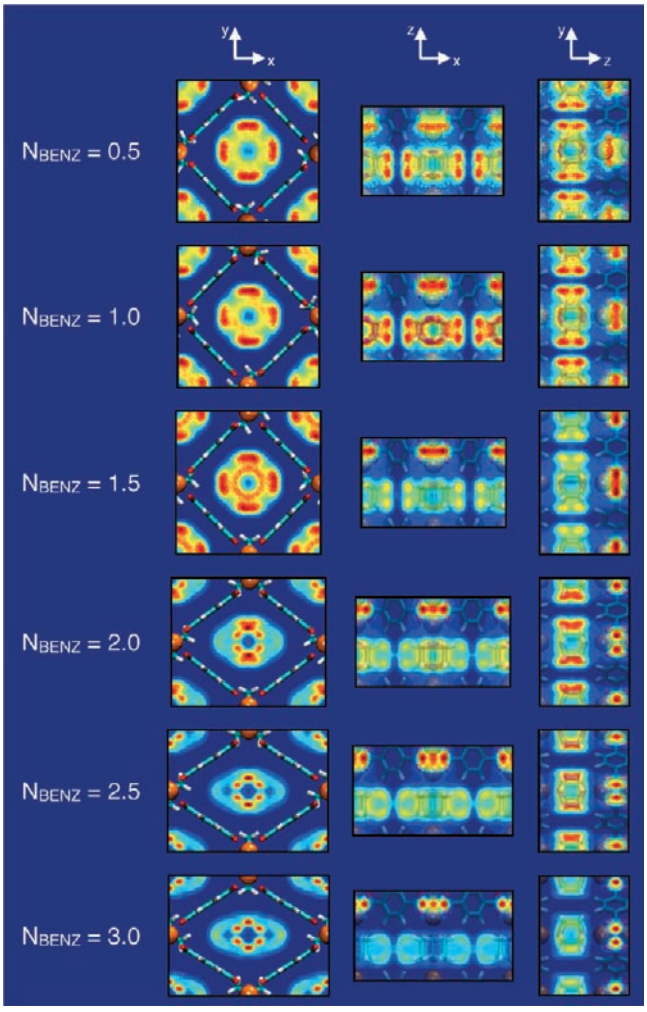

Figure 8. Two-dimensional density maps obtained as a function of the number of benzene molecules per unit cell by projecting the coordinates of the carbon atoms of each benzene molecule into the $x-y$ (left panels), $x-z$ (middle panels), and $z-y$ (right panels) planes that are defined in Figure 1. The density is normalized to the maximum value for each panel, and the color scheme varies from blue = 0.0 to red = 1.0.

effects of chemically different guests on the shape and size of the DMOF-1 pores, the adsorption of isopropyl alcohol was also investigated and compared to the available experimental data.[39,40] The first set of $N\sigma T$ simulations was carried out at T = 308 K for DMOF-1 with three IPA molecules per unit cell. These conditions were chosen to allow for a direct comparison with the experimental data of ref 39. The calculated a, b, and c unit cell vectors obtained by averaging over 3 ns of simulation are, respectively, 11.5 ± 0.2, 17.8 ± 0.2, and 9.68 ± 0.07 Å, which qualitatively reproduces the corresponding experimental values of 12.044, 16.112, and 9.316 Å. The present simulations thus predict an average DMOF-1 pore that is slightly narrower than that determined from the experimental measurements. However, the analysis of the structural changes of the DMOF-1 framework induced by a variable number of IPA molecules per unit cell, with N_{IPA} = 1.0−5.0, indicates that the calculated pore dimensions correlate nicely with the available experimental data.[39,40] In particular, the present simulations predict the existence of a narrow pore structure with three IPA molecules adsorbed per unit cell, while the large pore structure is found to

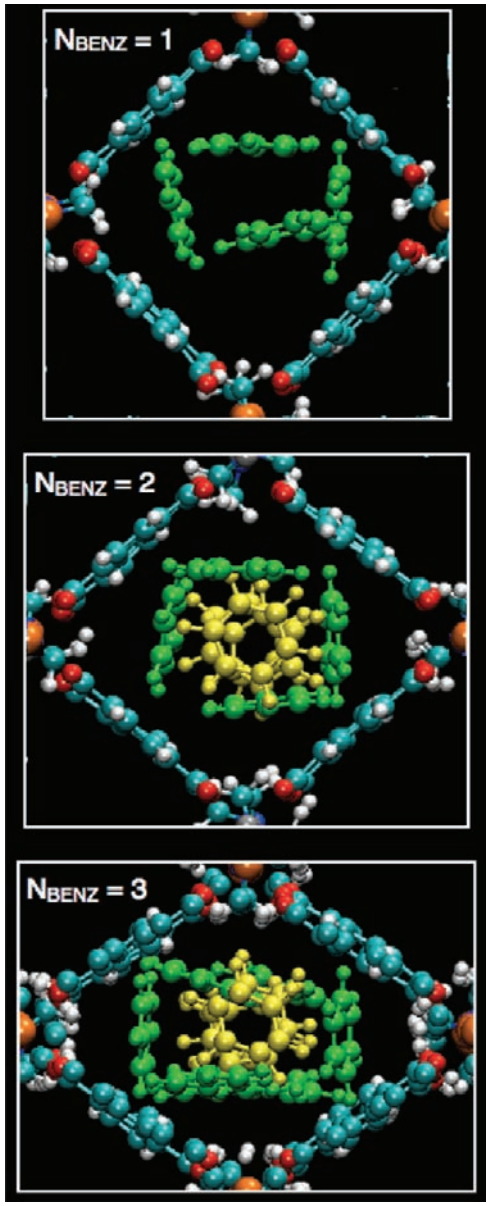

Figure 9. Three-dimensional snapshots along the c axis taken from $N\sigma T$ simulations of DMOF-1 at T = 223 K with N_{BENZ} = 1.00, 2.00, and 3.00. The benzene molecules lying on the $x-y$ plane are shown in yellow, while those lying parallel to the c axis are shown in green. The same color scheme as in Figure 1 is used for the atoms of the framework.

be the most stable configuration when $N_{IPA} \geq 4.0$. These results correctly reproduce the available experimental data that indicate the existence of NP and LP structures with N_{IPA} = 3.0 and N_{IPA} = 4.5, respectively. Figure 10 also shows that for N_{IPA} = 1 and 2, DMOF-1 exists in a LP configuration that undergoes the transition into the NP configuration as N_{IPA} increases to 3.0. Thus, unlike the results described above for the benzene adsorption, the present MD simulations predict that DMOF-1 undergoes two distinct structural transitions as a function of the amount of isopropyl alcohol adsorbed. Interestingly, a similar LP−NP−LP transition has also been predicted by simulations to occur in MIL-53 upon adsorption of CO_2 and H_2O.[30,35]

On the basis of the agreement between the simulation results and the experimental data of ref 39, related to the dependence of the DMOF-1 structure upon adsorption of a variable amount

dx.doi.org/10.1021/ja2100615 | J. Am. Chem. Soc. 2012, 134, 4207−4215

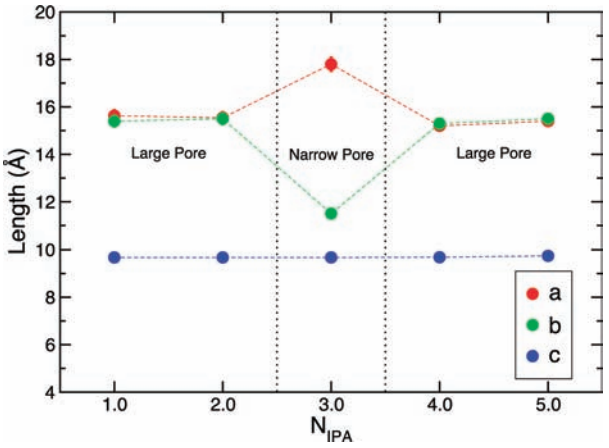

Figure 10. Variation of the unit cell vectors of DMOF-1 at T = 308 K as a function of the number of isopropyl alcohol molecules adsorbed per unit cell.

of isopropyl alcohol, it is thus likely that the differences between the experimentally determined and calculated pore dimensions are due to inaccuracies in the representation of the molecular interactions between the framework and IPA molecules. In this regard, it is important to note that, unlike the benzene force field, which has been accurately refined to reproduce high-level ab initio calculations of the benzene–benzene interactions,[60] no ab initio-based force field is currently available for isopropyl alcohol.

Fundamental insights into the different response of the DMOF-1 framework upon adsorption of chemically different species can be gained from the analysis of the spatial distribution of the IPA molecules within the pores. Figure 11 shows a series of two-dimensional density maps obtained by projecting the coordinates of the carbon atoms of each IPA molecules into the x–y (left panels), x–z (middle panels), and z–y (right panels) planes. Also shown as dark contours is the 2-D density associated with the oxygen atoms. For N_{IPA} = 1, the molecules are distributed in the center of the channels with the OH group pointing toward the metal units to form hydrogen bonds with the oxygen atoms of the two BDC ligands bound to the same Zn atom. As shown in the right panel of Figure 11, this particular orientation of the IPA molecules effectively leads to the formation of narrow hydrophobic channels within the DMOF-1 channels (see also Figure 12). A similar spatial arrangement of the IPA molecules is also found at N_{IPA} = 2, while a dramatic change occurs at N_{IPA} = 3. In this case, the IPA molecules are still located in the center of the channels but are now highly aligned, with their OH groups pointing mainly along the y-direction. The high directionality of the IPA OH groups, which now form hydrogen bonds with only the oxygen atoms of the BDC ligands that are bound to the metal units located along the y-axis, results in the collapse of the DMOF-1 structure into the narrow pore configuration. At N_{IPA} = 4, the DMOF-1 structure opens up again. As shown in Figure 11, this new structural transition can be directly related to the change in the spatial arrangement of the IPA molecules within the pores. The x–y density map indicates that the IPA molecules are still preferentially located in the center of the pores but are now parallel to the BDC ligands although shifted along the z-axis relative to them. Within this particular arrangement, each OH group of the IPA molecules forms only one hydrogen bond with one oxygen atom of a BDC ligand. The OH groups of the

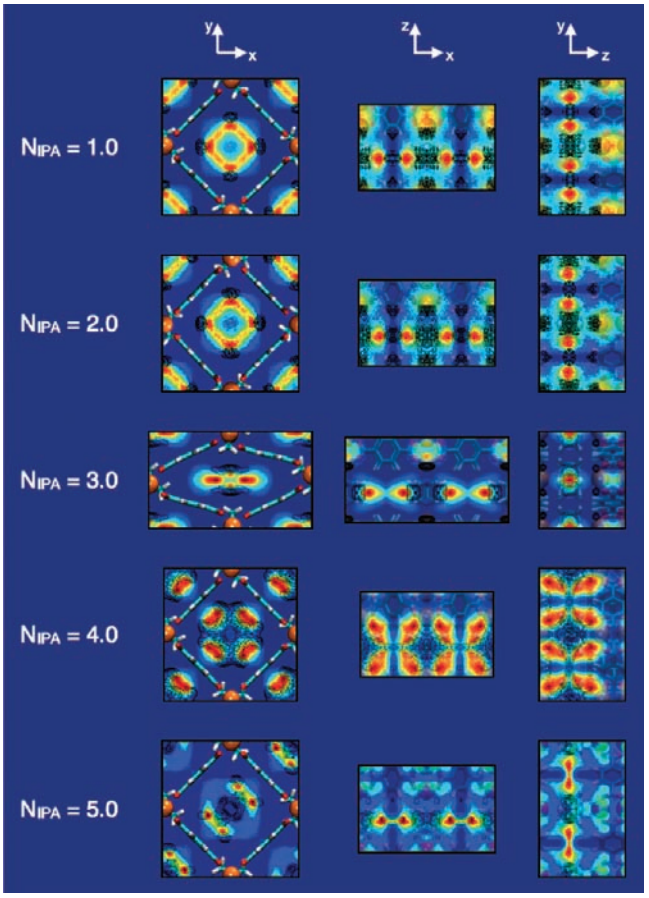

Figure 11. Two-dimensional density maps obtained as a function of the number of isopropyl alcohol molecules per unit cell by projecting the coordinates of the carbon atoms of each IPA molecule into the x–y (left panels), x–z (middle panels), and z–y (right panels) planes that are defined in Figure 1. The density is normalized to the maximum value for each panel, and the color scheme varies from blue = 0.0 to red = 1.0.

IPA molecules located in different pores are now more aligned, which can effectively result in the formation of weak hydrogen bonds through the gaps within the framework. Moreover, it is also possible to see that some of the IPA molecules point their OH groups toward the center of the channels. The additional hydrogen-bond interactions between these OH groups and the establishment of less directional hydrogen bonds with the framework effectively lead to the expansion of the structure, which thus results in the pore opening. A similar distribution of the IPA molecules within the DMOF-1 pores is also found at N_{IPA} = 5.0. In this case, it is possible to note that the IPA molecules are, on average, aligned along one particular diagonal of the pore, which may be related to the establishment of stronger hydrogen-bond interactions between molecules located in different pores. Snapshots taken from $N\sigma T$ simulations at three different IPA loadings are reported in Figure 12, which show the instantaneous arrangement of the molecules along the DMOF-1 channels.

The present MD results thus provide the first molecular-level explanation of the breathing behavior of DMOF-1 upon adsorption of isopropyl alcohol, which supports the analysis of the experimental data reported in refs 39 and 40. In particular, the simulation results provide clear evidence of the key role played by the hydrogen bonds established by the hydroxyl

dx.doi.org/10.1021/ja2100615 | J. Am. Chem. Soc. 2012, 134, 4207–4215

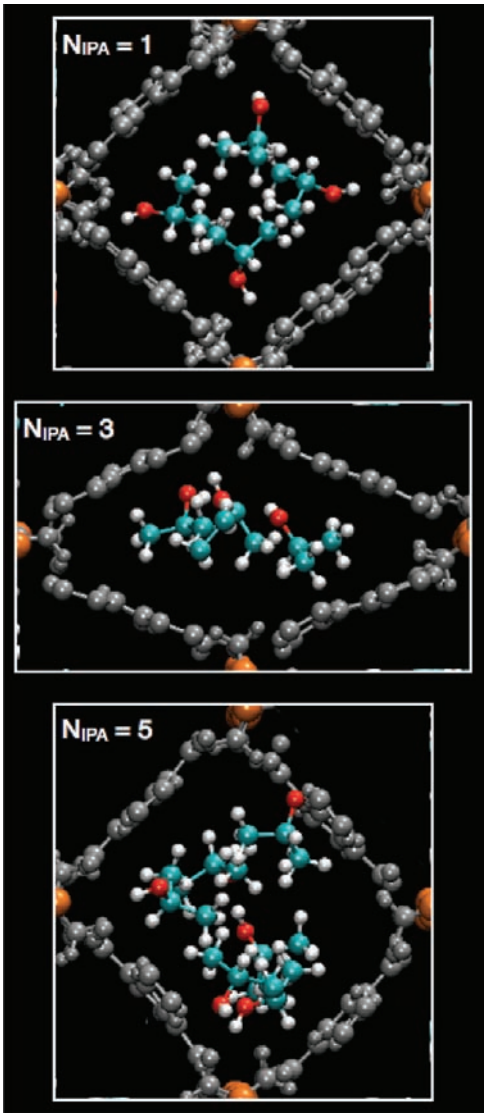

Figure 12. Three-dimensional snapshots along the *c* axis taken from $N\sigma T$ simulations of DMOF-1 at T = 308 K with N_{IPA} = 1.00, 3.00, and 5.00. For N_{IPA} = 1.00, four unit cells are used to show the preferential arrangement of the IPA molecules along the channel, while for N_{IPA} = 3.00 and 5.00, only IPA molecules belonging to one unit cell are shown. In all cases, the BDC and DABCO atoms are colored in gray, and the Zn atoms are shown in orange.

groups of the IPA molecules with the oxygen atoms of the BDC ligands in determining the structural LP−NP−LP transitions as a function of the number of IPA molecules adsorbed per unit cell. It is important to mention that the experimental data of ref 39 indicate the presence of more directional hydrogen bonds between IPA molecules located in different pores, which is only partially captured by the present MD simulations. This difference is likely related to inaccuracies in the description of the IPA interactions as well as to the different conditions that were used to obtain the crystal structure of DMOF-1 with IPA molecules.

4. CONCLUSIONS

The breathing behavior of the jungle-gym-type DMOF-1 metal−organic framework was studied through molecular dynamics simulations performed with a fully flexible model derived from ab initio calculations. The structural deformations induced by benzene and isopropyl alcohol were characterized at a molecular level as a function of temperature and loading. It was shown that for low benzene loadings ($N_{BENZ} \leq 2.00$) the most stable configuration of DMOF-1 is the open pore structure. The structural transition from LP to NP configurations occurs at N_{BENZ} = 2.00 and is driven by the interactions between the BDC ligands and the benzene molecules that lie perpendicularly to the channels. These molecules effectively act as gates that separate the individual pores. A temperature-dependent analysis of the breathing behavior of DMOF-1 upon benzene adsorption indicates that the NP structure corresponds to the most stable configuration at low temperature ($T \leq 223$ K), with the transition to the LP structure occurring in the temperature range 223 K < T < 248 K.

A different molecular mechanism is instead responsible for the breathing behavior of DMOF-1 upon adsorption of isopropyl alcohol, which results in two distinct structural transitions. At low loading (N_{IPA} = 1.0 and 2.0), DMOF-1 is predicted to be in the large pore structure. The first transition from LP to NP configurations occurs for 2.0 < N_{IPA} < 3.0 and is driven by the establishment of highly directional hydrogen bonds between the hydroxyl groups of the isopropyl alcohol molecules and the oxygen atoms of the BDC ligands. The second structural transition from NP to LP configurations occurs for 3.0 < N_{IPA} < 4.0 and is related the establishment of less directional hydrogen bonds between the IPA molecules and the framework as well as to the hydrogen-bond interactions between molecules located in the same pore.

In all cases, the structural parameters obtained from the simulations are in good agreement with the available experimental data, which provides support for the accuracy of the new flexible model in describing the molecular mechanisms that are responsible for the breathing behavior of DMOF-1. Hence, this study represents the first step toward the characterization of the modulation of the breathing behavior of DMOF-1 upon functionalization of the framework, which remains poorly understood in many respects.

■ ASSOCIATED CONTENT

Ⓢ Supporting Information

Full references for the main text, and details of the fitting procedure used in the development of the flexible force field for DMOF-1 including the complete list of force field parameters. This material is available free of charge via the Internet at http://pubs.acs.org.

■ AUTHOR INFORMATION

Corresponding Author

fpaesani@ucsd.edu

Notes

The authors declare no competing financial interest.

■ ACKNOWLEDGMENTS

This research was supported by start-up funds from the University of California at San Diego. We are grateful to the National Science Foundation for a generous allocation of computing time on Teragrid resources as well as to the San Diego Supercomputer Center for a computing time allocation on the Triton Computing Cluster through the TAPP program. We also thank Prof. Seth Cohen and Prof. Zhenqiang "Rick"

Wang for many helpful discussions on the breathing behavior of MOFs.

REFERENCES

(1) Ferey, G. *Chem. Soc. Rev.* **2008**, *37*, 191−214.
(2) Long, J. R.; Yaghi, O. M. *Chem. Soc. Rev.* **2009**, *38*, 1213−1214.
(3) Horike, S.; Shimomura, S.; Kitagawa, S. *Nat. Chem.* **2009**, *1*, 695−704.
(4) Ferey, G.; Serre, C.; Devic, T.; Maurin, G.; Jobic, H.; Llewellyn, P. L.; De Weireld, G.; Vimont, A.; Daturi, M.; Chang, J. S. *Chem. Soc. Rev.* **2011**, *40*, 550−562.
(5) Yaghi, O. M.; O'Keeffe, M.; Ockwig, N. W.; Chae, H. K.; Eddaoudi, M.; Kim, J. *Nature* **2003**, *423*, 705−714.
(6) Chae, H. K.; Siberio-Perez, D. Y.; Kim, J.; Go, Y.; Eddaoudi, M.; Matzger, A. J.; O'Keeffe, M.; Yaghi, O. M. *Nature* **2004**, *427*, 523−527.
(7) Millward, A. R.; Yaghi, O. M. *J. Am. Chem. Soc.* **2005**, *127*, 17998−17999.
(8) Rowsell, J. L. C.; Spencer, E. C.; Eckert, J.; Howard, J. A. K.; Yaghi, O. M. *Science* **2005**, *309*, 1350−1354.
(9) Britt, D.; Tranchemontagne, D.; Yaghi, O. M. *Proc. Natl. Acad. Sci. U.S.A.* **2008**, *105*, 11623−11627.
(10) Wang, B.; Cote, A. P.; Furukawa, H.; O'Keeffe, M.; Yaghi, O. M. *Nature* **2008**, *453*, 207−211.
(11) Britt, D.; Furukawa, H.; Wang, B.; Glover, T. G.; Yaghi, O. M. *Proc. Natl. Acad. Sci. U.S.A.* **2009**, *106*, 20637−20640.
(12) Li, Q. W.; Zhang, W. Y.; Miljanic, O. S.; Sue, C. H.; Zhao, Y. L.; Liu, L. H.; Knobler, C. B.; Stoddart, J. F.; Yaghi, O. M. *Science* **2009**, *325*, 855−859.
(13) Deng, H. X.; Doonan, C. J.; Furukawa, H.; Ferreira, R. B.; Towne, J.; Knobler, C. B.; Wang, B.; Yaghi, O. M. *Science* **2010**, *327*, 846−850.
(14) Doonan, C. J.; Tranchemontagne, D. J.; Glover, T. G.; Hunt, J. R.; Yaghi, O. M. *Nat. Chem.* **2010**, *2*, 235−238.
(15) Furukawa, H.; Ko, N.; Go, Y. B.; Aratani, N.; Choi, S. B.; Choi, E.; Yazaydin, A. O.; Snurr, R. Q.; O'Keeffe, M.; Kim, J.; Yaghi, O. M. *Science* **2010**, *329*, 424−428.
(16) Ferey, G.; Mellot-Draznieks, C.; Serre, C.; Millange, F.; Dutour, J.; Surble, S.; Margiolaki, I. *Science* **2005**, *309*, 2040−2042.
(17) Horcajada, P.; et al. *Nat. Mater.* **2010**, *9*, 172−178.
(18) Horcajada, P.; Serre, C.; Vallet-Regi, M.; Sebban, M.; Taulelle, F.; Ferey, G. *Angew. Chem., Int. Ed.* **2006**, *45*, 5974−5978.
(19) Zhao, D.; Timmons, D. J.; Yuan, D. Q.; Zhou, H. C. *Acc. Chem. Res.* **2011**, *44*, 123−133.
(20) Dybtsev, D. N.; Chun, H.; Kim, K. *Angew. Chem., Int. Ed.* **2004**, *43*, 5033−5036.
(21) Serre, C.; Millange, F.; Thouvenot, C.; Nogues, M.; Marsolier, G.; Louer, D.; Ferey, G. *J. Am. Chem. Soc.* **2002**, *124*, 13519−13526.
(22) Loiseau, T.; Serre, C.; Huguenard, C.; Fink, G.; Taulelle, F.; Henry, M.; Bataille, T.; Ferey, G. *Chem.-Eur. J.* **2004**, *10*, 1373−1382.
(23) Ramsahye, N. A.; Maurin, G.; Bourrelly, S.; Llewellyn, P. L.; Loiseau, T.; Serre, C.; Ferey, G. *Chem. Commun.* **2007**, 3261−3263.
(24) Horcajada, P.; Serre, C.; Maurin, G.; Ramsahye, N. A.; Balas, F.; Vallet-Regi, M.; Sebban, M.; Taulelle, F.; Ferey, G. *J. Am. Chem. Soc.* **2008**, *130*, 6774−6780.
(25) Llewellyn, P. L.; Maurin, G.; Devic, T.; Loera-Serna, S.; Rosenbach, N.; Serre, C.; Bourrelly, S.; Horcajada, P.; Filinchuk, Y.; Ferey, G. *J. Am. Chem. Soc.* **2008**, *130*, 12808−12814.
(26) Shimomura, S.; Horike, S.; Matsuda, R.; Kitagawa, S. *J. Am. Chem. Soc.* **2007**, *129*, 10990−10991.
(27) Shimomura, S.; Matsuda, R.; Kitagawa, S. *Chem. Mater.* **2010**, *22*, 4129−4131.
(28) Shimomura, S.; Higuchi, M.; Matsuda, R.; Yoneda, K.; Hijikata, Y.; Kubota, Y.; Mita, Y.; Kim, J.; Takata, M.; Kitagawa, S. *Nat. Chem.* **2010**, *2*, 633−637.
(29) Ferey, G.; Serre, C.; Mellot-Draznieks, C.; Millange, F.; Surble, S.; Dutour, J.; Margiolaki, I. *Angew. Chem., Int. Ed.* **2004**, *43*, 6296−6301.
(30) Salles, F.; Ghoufi, A.; Maurin, G.; Bell, R. G.; Mellot-Draznieks, C.; Ferey, G. *Angew. Chem., Int. Ed.* **2008**, *47*, 8487−8491.
(31) Ferey, G.; Serre, C. *Chem. Soc. Rev.* **2009**, *38*, 1380−1399.
(32) Wang, Z. Q.; Cohen, S. M. *J. Am. Chem. Soc.* **2009**, *131*, 16675.
(33) Boutin, A.; Coudert, F. X.; Springuel-Huet, M. A.; Neimark, A. V.; Ferey, G.; Fuchs, A. H. *J. Phys. Chem. C* **2010**, *114*, 22237−22244.
(34) Hamon, L.; Leclerc, H.; Ghoufi, A.; Oliviero, L.; Travert, A.; Lavalley, J. C.; Devic, T.; Serre, C.; Ferey, G.; De Weireld, G.; Vimont, A.; Maurin, G. *J. Phys. Chem. C* **2011**, *115*, 2047−2056.
(35) Salles, F.; Bourrelly, S.; Jobic, H.; Devic, T.; Guillerm, V.; Llewellyn, P.; Serre, C.; Ferey, G.; Maurin, G. *J. Phys. Chem. C* **2011**, *115*, 10764−10776.
(36) Devic, T.; et al. *J. Am. Chem. Soc.* **2010**, *132*, 1127−1136.
(37) Kim, M.; Boissonnault, J. A.; Dau, P. V.; Cohen, S. M. *Angew. Chem., Int. Ed.* **2011**, *50*, 12193−12196.
(38) Karra, J. R.; Walton, K. S. *J. Phys. Chem. C* **2010**, *114*, 15735−15740.
(39) Uemura, K.; Yamasaki, Y.; Komagawa, Y.; Tanaka, K.; Kita, H. *Angew. Chem., Int. Ed.* **2007**, *46*, 6662−6665.
(40) Uemura, K.; Yamasaki, Y.; Onishi, F.; Kita, H.; Ebihara, M. *Inorg. Chem.* **2010**, *49*, 10133−10143.
(41) Rosenbach, N.; Jobic, H.; Ghoufi, A.; Salles, F.; Maurin, G.; Bourrelly, S.; Llewellyn, P. L.; Devic, T.; Serre, C.; Ferey, G. *Angew. Chem., Int. Ed.* **2008**, *47*, 6611−6615.
(42) Chen, Y. F.; Lee, J. Y.; Babarao, R.; Li, J.; Jiang, J. W. *J. Phys. Chem. C* **2010**, *114*, 6602−6609.
(43) Nijem, N.; Thissen, P.; Yao, Y.; Longo, R. C.; Roodenko, K.; Wu, H.; Zhao, Y.; Cho, K.; Li, J.; Langreth, D. C.; Chabal, Y. J. *J. Am. Chem. Soc.* **2011**, *133*, 12849−12857.
(44) Coombes, D. S.; Cora, F.; Mellot-Draznieks, C.; Bell, R. G. *J. Phys. Chem. C* **2008**, *113*, 544−552.
(45) Coudert, F. X.; Jeffroy, M.; Fuchs, A. H.; Boutin, A.; Mellot-Draznieks, C. *J. Am. Chem. Soc.* **2008**, *130*, 14294−14302.
(46) Coudert, F. X.; Mellot-Draznieks, C.; Fuchs, A. H.; Boutin, A. *J. Am. Chem. Soc.* **2009**, *131*, 3442−3443.
(47) Coudert, F. X.; Boutin, A.; Jeffroy, M.; Mellot-Draznieks, C.; Fuchs, A. H. *ChemPhysChem* **2011**, *12*, 247−258.
(48) Dubbeldam, D.; Krishna, R.; Snurr, R. Q. *J. Phys. Chem. C* **2009**, *113*, 19317−19327.
(49) Case, D. A.; Wang, J. M.; Wolf, R. M.; Caldwell, J. W.; Kollman, P. A. *J. Comput. Chem.* **2004**, *25*, 1157−1174.
(50) Frisch, M. J.; et al. *Gaussian 09*, revision A.1; Gaussian, Inc.: Wallingford, CT, 2009.
(51) Zhao, Y.; Truhlar, D. G. *Theor. Chem. Acc.* **2008**, *120*, 215−241.
(52) Becke, A. D. *J. Chem. Phys.* **1993**, *98*, 5648−5652.
(53) Dunning, T. H. Jr. *J. Chem. Phys.* **1989**, *90*, 1007.
(54) Hay, P. J.; Wadt, W. R. *J. Chem. Phys.* **1985**, *82*, 270.
(55) Peterson, K. A.; Puzzarini, C. *Theor. Chem. Acc.* **2005**, *114*, 283−296.
(56) Breneman, C. M.; Wiberg, K. B. *J. Comput. Chem.* **1990**, *11*, 361−373.
(57) Tafipolsky, M.; Amirjalayer, S.; Schmid, R. *J. Phys. Chem. C* **2010**, *114*, 14402−14409.
(58) Chen, Z. X.; Xiang, S. C.; Zhao, D. Y.; Chen, B. L. *Cryst. Growth Des.* **2009**, *9*, 5293−5296.
(59) Jorgensen, W. L.; Severance, D. L. *J. Am. Chem. Soc.* **1990**, *112*, 4768−4774.
(60) Sherrill, C. D.; Sumpter, B. G.; Sinnokrot, M. O.; Marshall, M. S.; Hohenstein, E. G.; Walker, R. C.; Gould, I. R. *J. Comput. Chem.* **2009**, *30*, 2187−2193.
(61) Todorov, I. T.; Smith, W. C.; Trachenko, K.; Dove, M. T. *J. Mater. Chem.* **2006**, *16*, 1611−1618.
(62) Frenkel, D.; Smit, B. *Understanding Molecular Simulation: From algorithms to applications*; Academic Press: New York, 2001.